International Journal of Thermal Sciences 122 (2017) 172–185

Contents lists available at ScienceDirect

International Journal of Thermal Sciences

journal homepage: www.elsevier.com/locate/ijts

Augmentation of convective heat transfer in the cooling zone of brick tunnel kiln using guide vanes: An experimental study

H.A. Refaey*, Ali A. Abdel-Aziz, R.K. Ali, H.E. Abdelrahman, M.R. Salem

Department of Mechanical Engineering, Faculty of Engineering at Shoubra, Benha University, 11629 Cairo, Egypt

ARTICLE INFO

Article history:
Received 1 May 2017
Received in revised form
15 July 2017
Accepted 21 August 2017

Keywords:
Tunnel kiln
Experiments
Convective
Augmentation technique
Guide vanes

ABSTRACT

One of the most important priorities in brick industry is to reduce energy consumption. Therefore, the present work aims to enhance the average Nusselt number that provides an indication of the production time of the tunnel kiln. A test rig simulating the cooling section of tunnel kiln, by scale 1:4 has been designed and fabricated. Augmentation technique using guide vanes with attack angles ($\theta = 120^\circ$, 135°, and 150°) in flow direction are attached to the side walls to direct the flow toward the confined zone between the heated columns. This technique is applied on ten different settings within Reynolds number range of $11{,}867 \leq Re \leq 25{,}821$. The results demonstrate that the heat transfer and pressure drop depends on the brick setting. Furthermore, using guide vanes increases the heat transfer rates with all settings. The maximum enhancement of about 94.5% is obtained for longitudinal brick at middle column (compared with that nearest to the wall) in setting 2 at $\theta = 135^\circ$ and $Re = 22{,}407$. Finally, the present study aimed to extend kiln designers with Nusselt number correlations within $11{,}867 \leq Re \leq 25{,}821$, $0.33 \leq (S/a) \leq 1.0$, $0.79 \leq (\varepsilon S/b) \leq 3.0$, and $120^\circ \leq \theta \leq 180^\circ$.

1. Introduction

Tunnel kilns are widely used in ceramic and brick manufacturing industries. A tunnel kiln consists of a series of connected counter current heat exchangers with the solids on the kiln car which moving continuously in the opposite direction of the air flow. The kiln has three main temperature zones; preheating, firing and cooling. Tunnel kiln has a typical length between 35 m and 250 m and its width varies from 1 m to 6 m [1,2]. The green ware entering the preheating zone encounters the hot exhaust gases from the downstream firing zone. Thus the green ware is heated whereas the exhaust gases cool down leaving the tunnel kiln with a relatively low temperature.

The green ware continues on to the firing zone where fuel is introduced to heat the product up to the required sintering temperature. Then, the hot product moves to the cooling zone, where it gives off some of its heat to the cooling air as it passes in the opposite direction. Fig. 1 reveals schematic diagram of temperature distribution along tunnel kiln. Many studies have been done to improve the various aspects of kilns such as firing systems [3,4], decking process [5–7], reducing false air [8], edge and roof gaps [9] and pollution control [10–12].

The intensive energy consumption in fire brick industry forced many researchers to study the thermal problem inside tunnel kilns [13–29]. Dugwell and Oakley [13] investigated the heat transfer process in tunnel kilns where they represented the whole column of bricks by a solid chrome magnesite block. The authors measured the heat transfer between air and sides, top and back of the column. The brick column was treated as a solid block ignoring the actual hydrodynamic pattern around the bricks in the column, which was the main drawback of that study. Karaush et al. [14] conducted an experimental study involving a model unit on heat absorption from the radiating walls of a kiln by the ceramic ware set up on a kiln car. They concluded that there is always optimal spacing between the ceramic pieces in the setting above which any further increase in the spacing would not increase the rate of heat absorption by the ware.

Abou-Ziyan [15] investigated experimentally the thermal performance in the cooling section of a tunnel kiln, for a wide range of Reynolds numbers from 6000 to 33,000 and six different settings arrangements of bricks. The results showed that the pressure drop and convective heat transfer coefficient strongly depends on the setting pattern. Correlations predicting of the pressure drop and heat transfer for refractory materials were obtained in the form of

* Corresponding author.
E-mail address: hassanein.refaey@feng.bu.edu.eg (H.A. Refaey).

http://dx.doi.org/10.1016/j.ijthermalsci.2017.08.018
1290-0729/

Nomenclature

a	Brick length, mm
A	Area, m^2
B	Brick width, mm
c	Brick height, mm
Cp	Specific heat , J/kg.K
D	Diameter, m
f	Friction factor
h	Convective heat transfer coefficient,$W/m^2.K$
H	Duct height, mm
I	Electric current, Amp
k	Fluid thermal conductivity, W/m.K
L	Length of brick setting, mm
M	Mass flux, $kg/s.m^2$
Nu	Average Nusselt number
P	Pressure, Pa
Q	Heat transfer rate, W
Qinput	Input heat from variac, W
Re	Reynolds number
S	Spacing between columns, mm
T	Temperature, K
u	Superficial velocity, m/s
U	Interstitial velocity, m/s
V	Volume, m^3
Vi	Voltage drop, Volt
W	Duct width, mm

Greek letters

θ	Attack angle
ε	Void fraction
ρ	Density, kg/m^3
ρ_s	Setting density $= V_b/V_d$
ω	Uncertainty
η	Performance criteria
ν	Kinematic viscosity, m^2/s
Ω	Ohm

Subscript

a, b	Air bulk temperature
a m, o	Average temperature at outlet
a m, i	Average temperature at inlet
a, i	Thermocouple readings at inlet
ave	Average value
b	Brick
i	Local value
s,i	Local brick surface temperature
d	Duct
f	Flow
h	Hydraulic
w	Wet area
w, b	Bricks wet area
w, d	Duct wet area
mv	Middle with vanes
w,nv	Wall with no vanes

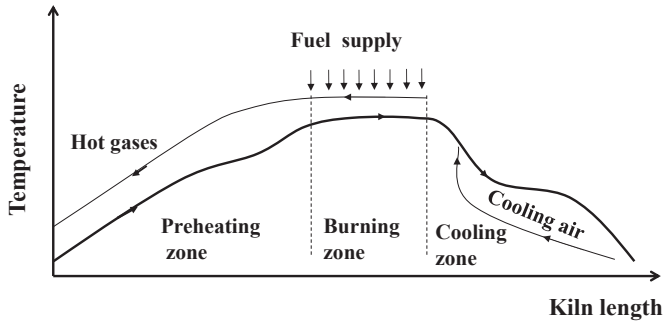

Fig. 1. Schematic diagram of temperature distribution along tunnel kiln [1,2].

friction factor and Nusselt number as functions of Reynolds number, voidage, column spacing to brick thickness and column spacing to brick length. Carvalho and Nogueira [17] reported that the numerical simulation is a good tool for the development of an optimization procedure to be used in the kiln design and operation. Almeida et al. [20] presented a mathematical model and numerical solution to describe the drying of ceramic hollow bricks in a tunnel dryer of cross flow type on an industrial scale. Results of moisture content and temperature of the product, temperature, relative humidity and humidity ratio of drying air as a function of drying time and bed length of the dryer are presented and analyzed. Refaey and Specht [21] presented 3D analysis for the preheating zone to simulate the effect of nozzle axial velocity and its arrangement. Their results showed that the effect of cross-sectional velocity was much higher than the axial velocity. As a consequence, the radial velocity produced by the burner and the nozzles was necessary to increase the heat transfer. Mancuhan et al. [22] developed a one-dimensional model describing the gas flow, heat transfer between gas and bricks and evaporation of bound water in the preheating zone of a tunnel kiln. Their study aimed to feed ambient air into the preheating zone using two different profiles and vent locations. The results showed that when no ambient air was fed, the gas temperature reaches 350 °C at the preheating zone entrance which was not desired for the best product quality. Kaya et al. [23] developed a mathematical model representing the phenomena of heat transfer and fluid flow to compute air mass flow rate, brick and air temperatures along the cooling zone of a tunnel kiln. The results showed that the minimum pressure drop was obtained by considering the tunnel kiln cooling zone composed of two regions with a suction flow and the two other regions of blowing type. Nicolau et al. [24] presented a numerical and experimental thermal analysis of a tunnel kiln used in ceramic production. They introduced three-dimensional temperature distribution within the walls, gas, and load along the kiln and a complete thermal energy balance including all energy fluxes related to the process. Durakovic and Delalic [25] developed a mathematical model for analysis and checking of a stationary temperature field in brick products and in the furnace. Naccache et al. [26] investigated numerically fluid flow and heat transfer of combustion gases inside a tunnel kiln using natural gas instead of sawdust. The effects of porosity, permeability and gasses inlet temperature were investigated and compared with experimental results from the literature. Their results showed that natural gas can be applied in a tunnel kiln. Essenhigh [27] performed an integral analysis of the energy equation through a tunnel kiln, to determine the relation between input energy and useful output energy.

Santos [28] presented a numerical formulation to obtain the thermal behavior of a tunnel kiln, considering the heat transfer among its several components. A good agreement between the numerical and experimental results was obtained for sawdust as a fuel. Numerical simulations with natural gas were also performed to evaluate its use as a fuel in this kind of kiln. Refaey et al. [1,29]

developed one-dimensional mathematical model for three different cases by using MATLAB program to predict temperature profile of gas and solid in tunnel kilns. Moreover, they studied the influence of fuel distribution along the firing zone. The results showed that, up to approximately 30% of the firing zone, the energy consumption was increased then there was a low increase in energy after that length.

The main objective of the present experimental investigation is to propose guide vanes strategy that can augment heat transfer and monitor the associated pressure drop in the brick tunnel kiln. The investigation is performed for turbulent flow in a simulated test section with 1:4 scale of the actual tunnel kiln. Ten brick settings were suggested, constructed, and tested by using a suction tunnel kiln. The temperature measurements were carried out on four typical brick models with different orientations in middle and side wall columns. Effects of brick setting-pattern and characteristics (columns spacing and brick spacing) on heat transfer rate and pressure drop are examined for ten different settings within Reynolds number ranging from 11,867 to 25,821 and three guide vanes attack angles (150^o, 135^o, and 120^o). The present experiments aimed to extend kiln designers with Nusselt number correlations as a function of longitudinal spacing ratio, transversal spacing ratio, vane attack angle, and Reynolds number.

2. Experimental test rig

A turbulent flow heat transfer characteristics through a tunnel kiln with different brick model settings are the present work objectives. Fig. 2 shows the schematic diagram of test rig of tunnel kiln flow system used in this work. The apparatus used in this study comprises a tunnel kiln flow system that consists of a suction-type air blower (4.1 kW), flow orifice meter, transition duct, test section with different brick model settings, main entrance duct, straightener, and bell-mouth intake. A variable gate area at the discharge outlet of the blower is used to control the air flow rate exhausted into the atmosphere. The working test section of the tunnel kiln has a cross section 350 mm width (W), 250 mm height (H), and 1500 mm long. The test section was made from 1.5 mm thick mild steel sheet and insulated with 25 mm glass wool to minimize the heat loss to the surrounding. A uniform air flow enters the test section through a bell mouth intake and then through the straightener before the transition duct to eliminate the swirl of the air flow. The transition duct was used to connect the blower circular tube and exit of the test section as shown in Fig. 2. A mild steel cover, hinged at the top side of the test section, is used to allow replacement of the bricks and guide vanes, and then closing the test section during experiments. The guide vanes are also made of mild steel sheet with different attack angles of 120°, 135° and 150° to the flow direction, attached to the two vertical walls of the tunnel. The guide vane has a length of 250 mm equal to the tunnel height, base width 20 mm, and height 20 mm. Top view of half of setting 2 with guide vanes is shown in Fig. 3a.

Guide vanes are mounted on the two side vertical walls of the test section to direct the flow towards the confined zone behind columns. Four heating elements of typical brick models were made of refractory brick and have the same dimension as the bricks in the settings. A nickel-chrome wire of 0.2 mm diameter and 10 Ω/m is wound helically in the brick heater and cheesed in a stainless steel probe to provide a constant heat flux condition. Fig. 3b shows the construction of the heating brick model. The used bricks dimensions and columns spacing are shown in Fig. 3a. Each setting is identified by three parameters, namely: layers, columns, and rows. Layers are the number of bricks in the vertical direction and there are eight layers for each setting in the present work. Columns are perpendicular to flow direction and the space between two columns is (S) as shown in Fig. 3a. Rows are in the flow direction and have a constant spacing of 30 mm as shown in Fig. 4. Each brick model setting is located downstream the bell mouth intake at a distance 5.0 of hydraulic diameter and the guide vanes are mounted on the two vertical walls of the test section. Fig. 3 represents a schematic of one row for each setting in the ten used settings. The measurements are taken conducted in the fifth raw [9,15]. For all of the present settings, the longitudinal and transversal heating elements for middle and near wall columns are located in layer 3 and 6 respectively as shown in Fig. 4.

Six K-type thermocouples (wires of 0.2 mm diameter) are directly inserted into the flow stream at inlet and exit of the test section (at three equally distanced positions from the top cover) to measure the air inlet and outlet temperatures. In addition to, another eight K-type thermocouples are used for measuring the heating brick surfaces temperature by embedding two thermocouples on both sides of each brick model. All thermocouples are calibrated in the laboratory against a mercury-in-glass thermometer, which could be accurately read to ±0.5 K. The thermocouples were connected to fifteen channels data acquisition system to record the temperatures. A digital differential pressure transducer (Dwyer® series WWDP with an accuracy of ±2% of full scale) is employed for measuring the static pressure drop of the air between the test section inlet and outlet through two taps of 2 mm diameter at mid-plane of the tunnel bottom surface. Ten different settings were constructed with different arrangements and spacing between columns as shown in Fig. 4. The characteristic dimensions of the different configurations are revealed in Table 1. All settings are examined within Reynolds number range of 11,867 to 25,821.

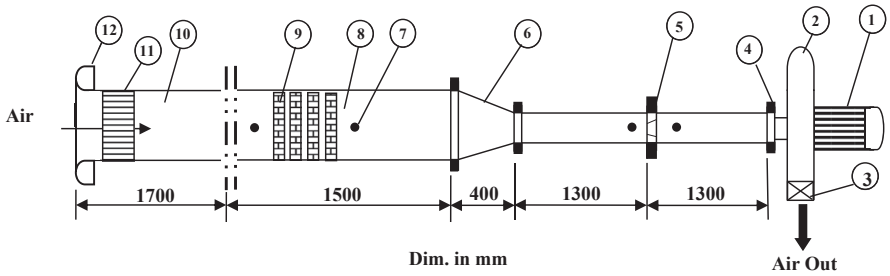

Fig. 2. Schematic diagram of the experimental test rig.

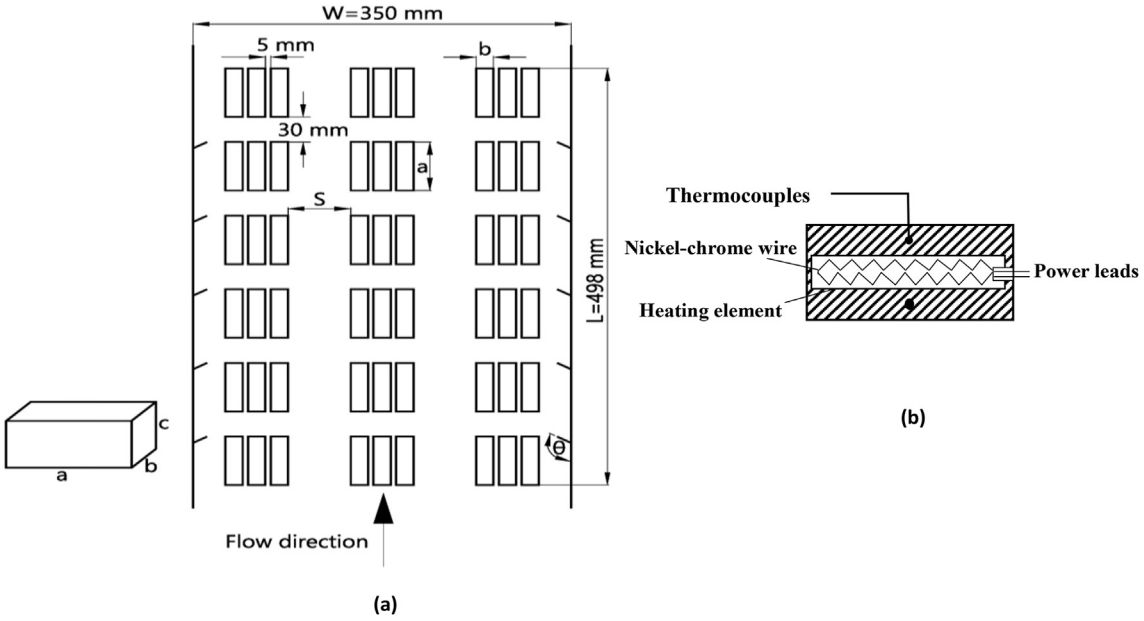

Fig. 3. (a) Top view details of setting 2 with guide vane angle 120°. (b) Cross section in a heating brick model.

3. Experimental procedures

The experimental procedures are initiated after assembling the following equipment: the suction-type air tunnel with its different parts (the electric motor, air blower, air gate controller, orifice meter, flanges, transition duct, test section duct, main entrance duct, straightener and bell-mouth intake), the thermocouples and the differential pressure transducer. The first step to collect the data from the system is loading the bricks in the test section and arranged according to the tested setting characteristics, and installing the guide vanes. The heaters and the electric motor were operated. The voltage drop and the electrical current are fixed at 8 ± 0.1 V and 2.9 ± 0.1 Amp, respectively. Then, the air velocity is adjusted by regulating the calibrated air gate controller. Furthermore, the consumed power by the heaters is adjusted by the voltage regulator. All outputs of the thermocouples and differential pressure transducer are recorded in Excel sheets on Laptop via the data acquisition system.

Totally, a series of 240 experiments was carried out on the ten bricks settings; 180 runs for the settings with guide vanes and 60 runs for no vanes. During the test operation, the steady-state condition is conducted when a maximum variation of 0.5 K for each thermocouple reading. Moreover, it is considered to be achieved when the stable fluid inlet and outlet temperatures are obtained; variation of inlet and outlet temperatures of the air stream were within 0.1 K during a minute period before each measurement was taken.

4. Data reduction

Excel sheets were prepared to process the experimental data for the heat transfer coefficients and pressure drop. It should be noted that for all calculations, the thermo-physical properties of the air in the test section are calculated at the bulk temperatures, $T_{a,b}$.

$$T_{a,b} = (T_{a,m,i} + T_{a,m,o})/2 \quad (1)$$

The mean temperature of the air at test section inlet and exit are calculated as the arithmetic mean of the local measurements.

4.1. Heat transfer calculations

The primary measurements in heat transfer calculations consist of seventeen variables, namely the flow rate, the inlet and outlet temperatures of air and the heating brick surface temperatures in addition to the voltage drop and the passed current through the heaters. The input power to the heater (Q_{input}) is regulated with 1 kW AC transformer and can be calculated from;

$$Q_{input} = V_i I \cos\varnothing \quad (2)$$

According to Ministry of electricity and energy in Egypt, the power factor, cos∅, for the public network is ranged from 0.93 to 0.97. In the present study, the AC power factor is assumed to be 0.95.

Neglecting any heat gain or loss, the consumed power by the heaters are assumed to be equal to the rate of heat transferred to the flowed air. From this energy balance, the local convective heat transfer coefficient, h_i is calculated as follows:

$$h_i = \frac{Q_{input}}{A_b(T_{s,i} - T_{a,b})} \quad (3)$$

It should be noted that the index i refers to either transversal or longitudinal brick in the middle or near the wall. Now, the average heat transfer coefficient can be calculated using Eq. (4);

$$h_{ave} = \frac{\sum h_i A_i}{\sum A_i} \quad (4)$$

The air velocity measured in the empty test section is called superficial velocity (u), which is obtained from the calibrated Orifice meter. However, the interstitial velocity (U) in each setting is calculated from;

$$U = \frac{u}{\varepsilon} \quad (5)$$

The void fraction (ε) of the setting is calculated from;

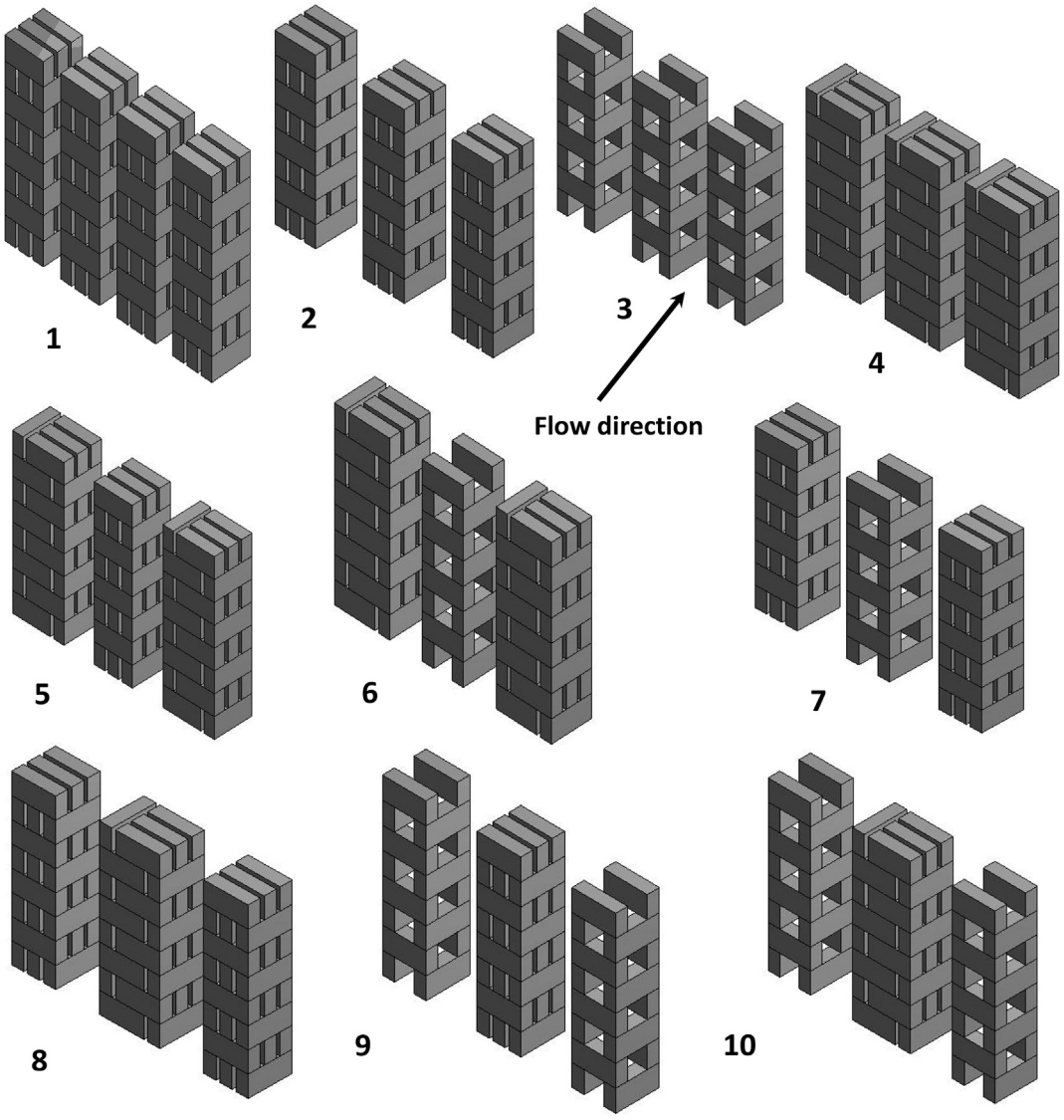

Fig. 4. Schematic representation of one row from each pattern of the ten different investigated settings.

Table 1
Characteristics of the tested settings.

Setting	No. of Bricks	ε	D_h (mm)	$A_{w,b}$ (m^2)	$A_{w,b}/A_{w,b1}$ (%)	$\rho_s = V_b/V_d$	S (mm)	S/a	S/b
1	576	0.6565	36.4	2.6150	100.0	0.3435	19.3	0.3333	1.2083
2	432	0.7424	51.6	1.9613	75.0	0.2576	58.0	1.0000	3.6250
3	288	0.8283	72.2	1.4365	54.9	0.1717	58.0	1.0000	3.6250
4	576	0.6565	37.1	2.5546	97.7	0.3435	26.5	0.4569	1.6563
5	528	0.6852	41.3	2.3568	90.1	0.3148	37.0	0.6379	2.3125
6	480	0.7138	45.7	2.1819	83.4	0.2862	37.0	0.6379	2.3125
7	384	0.7710	57.4	1.7864	68.3	0.2290	58.0	1.0000	3.6250
8	480	0.7138	46.1	2.1590	82.6	0.2862	47.5	0.8190	2.9688
9	336	0.7996	64.2	1.6115	61.6	0.2004	58.0	1.0000	3.6250
10	384	0.771	56.9	1.8092	69.2	0.2290	47.5	0.8190	2.9688

*The brick dimensions are a = 58 mm, b = 16 mm and c = 28 mm ρ_s is the setting density.

$$\varepsilon = \frac{V_f}{V_d} \tag{6}$$

The flow volume in each setting is the difference between duct and brick volume is calculated from;

$$V_f = V_d - V_b \tag{7}$$

The interstitial velocity is used to determine the flow regime through the bricks by calculating the Reynolds number which is based on the hydraulic diameter of the duct as follows;

$$Re = \frac{UD_h}{\nu} \tag{8}$$

Hydraulic diameter of the duct, D_h , for the different settings

according to the free volume and wet area as;

$$D_h = \frac{4V_f}{A_w} \quad (9)$$

And the wet area is calculated from the following equation;

$$A_w = A_{b,w} + A_{d,w} \quad (10)$$

Then the local, Nu_i, and average, Nu_{ave}, Nusselt numbers can be obtained as follows;

$$Nu_i = \frac{h_i D_h}{k} \quad (11)$$

$$Nu_{ave} = \frac{h_{ave} D_h}{k} \quad (12)$$

Where, k is the air thermal conductivity, W/(m.K).

4.2. Friction factor calculation

In the present study, the measurement of the friction factor was conducted at the same time as the heat transfer measurements to show the effect of different settings geometrical parameters at different operating conditions. The Darcy friction coefficient for the air in circulation inside the duct is calculated with the following equation;

$$f = \frac{2\Delta P\ D_h}{L\ \rho\ U^2} \quad (13)$$

5. Uncertainty analyses

In general, the accuracy of the experimental results depends on the accuracy of the individual measuring instruments and techniques. The uncertainty (ω) in the measured bricks and duct dimensions was assumed to be ±0.5 mm; this is guessed quantity from meter scale. In addition to, the uncertainty applied to the thermal properties of air is assumed to be ±0.1%. The uncertainty of the parameters is calculated based upon the root sum square combination of the effects of each of the individual inputs as introduced by Kline and McClintock [30]. For example, the uncertainty for the average *Nu* was estimated as follows;

$$\frac{\omega_{Nu_{ave}}}{Nu_{ave}} = \pm\sqrt{\left(\frac{\omega_{h_{ave}}}{h_{ave}}\right)^2 + \left(\frac{\omega_{D_h}}{D_h}\right)^2 + \left(\frac{\omega_k}{k}\right)^2} = \pm 3.3\ \% \quad (14)$$

For all experimental runs, the average uncertainties in main parameters are summarized in Table 2.

Table 2
Average uncertainties in main parameters.

Parameter	Uncertainty (ω)
h_{ave}	±1.6%
Nu_{ave}	±3.3%
u	±1.6%
U	±2.3%
Re	±3.7%
ΔP	±3.6%
f	±5.3%
Q	±2.12%

6. Results and discussion

6.1. Experimental validation

Firstly, primary experiments have been done with the same condition as those taken in Abo-Ziyan [15]. Fig. 5 introduces a comparison of the experimental data of local Nusselt number in the different position with the results of Abo-Ziyan [15] without vanes for setting 1. The maximum error did not exceed 10.5% that observed in the transversal middle as shown in Fig. 5. The obtained low values of the average uncertainties and the good agreement with previous studies revealed the confidence in the experimental setup and the used measurement techniques.

6.2. Local Nusselt number

Experimental results include the effects of the wall, the spacing between columns, and the spacing bricks on the local Nusselt number for longitudinal and transversal bricks in different settings are represented. Fig. 6 shows experimentally the local variation of Nusselt number (*Nu*) against Reynolds number for setting 2 in absence and presence of vanes with attack angles (θ = 120°, 135°, and 150°) in the direction of the main flow. For all longitudinal and transversal bricks, the values of *Nu* increases as Re increases for all settings with and without vanes.

In addition to, for all values of Re and attack angle (θ), the longitudinal brick at middle column has the best cooling and highest *Nu* in comparison with bricks in other positions. This can be attributed to the flow velocity on both sides of the longitudinal brick is higher than that of the transversal brick, which may exhibit flow separation and stagnation zone behind it.

The variation of local Nusselt number with Reynolds number for setting 7 is presented in Fig. 7. The local distributions of *Nu* in absence and presence of vanes with attack angles (θ = 120°, 135°and 150°) have almost the same trend as those for setting 2. The local Nusselt numbers that were obtained for setting 7 were greater than that was obtained by other settings in the absence and in presence vanes for different values of attack angles and Re as shown in Fig. 7. The increasing in heat transfer rate (local *Nu*) in setting 7 may be attributed to the combined effect of the high turbulence level (produced by vanes) and the low flow resistance around the bricks.

6.2.1. Effect of setting characteristics

1- Wall Effect

To show the wall effect, the results of the first four settings 1, 2, 3 and 4 could be analyzed. The experimental results are presented in the form of relative local Nusselt number or enhancement ratio percentage $[(Nu_{mv} - Nu_{w,nv})/Nu_{w,nv}]$ where Nu_{mv} is the local Nusselt number of longitudinal brick in middle in presence of side wall vanes and $Nu_{w,nv}$ is the local Nusselt number of longitudinal brick nearest to side wall in absence of side wall vanes. The relative local Nusselt number $[(Nu_{mv} - Nu_{w,nv})/Nu_{w,nv}]$ of longitudinal middle position have higher values (maximum enhancement) in presence of vanes with θ = 120° than those for 135° and 150° for settings 1, 3, and 4 within the investigated range of Re as can be seen in Table 3. For the four settings, it is observed that the relative local Nusselt numbers in absence of guide vanes are lower than that in presence of vanes with different attack angles as shown in Table 3. The maximum enhancement of about 94.5% is obtained for longitudinal brick at middle column (compared with that nearest to the wall) in setting 2 at θ = 135° when Re = 22,407 while a minimum enhancement of about 5.4% is obtained for setting 4 in absence of vanes at Re = 24,956. This occurs because the vanes produce high turbulence level due to the generated large-scale vortices along their trailing edges for θ = 135° much more likely than those for

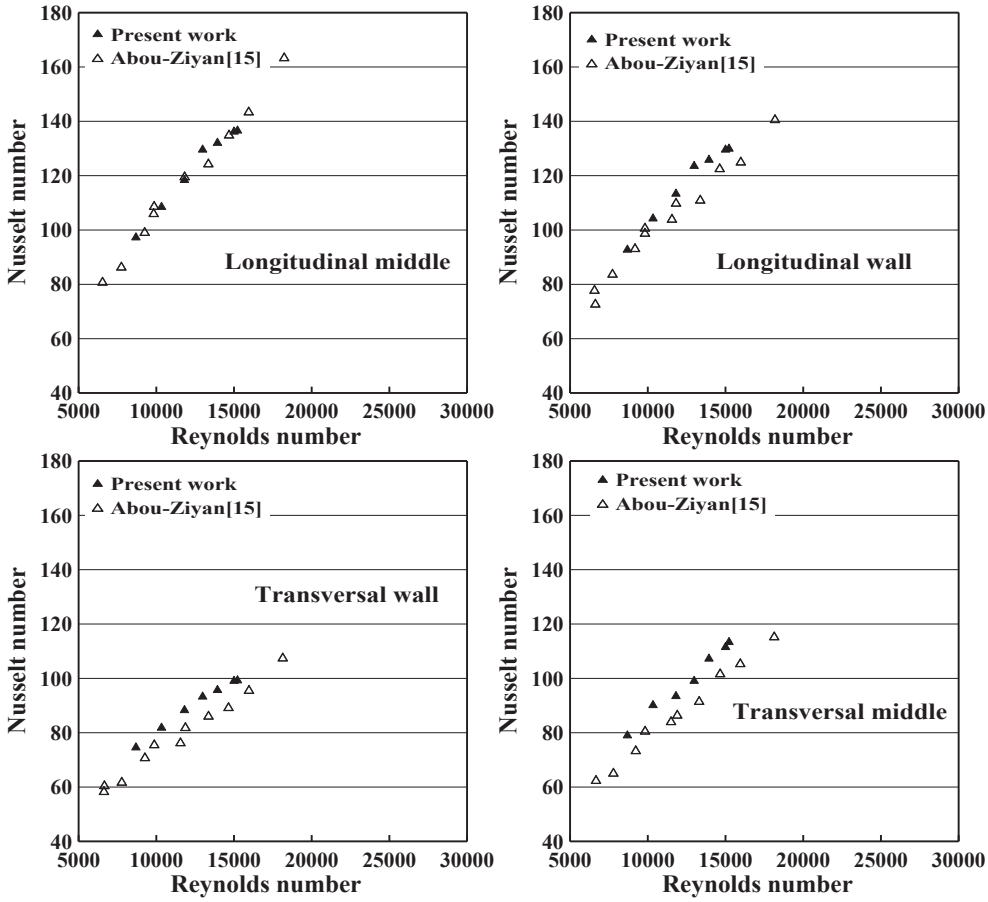

Fig. 5. Validation of the experimental local Nusselt number with previous results of Abo-Ziyan [15] for setting 1 without guide vanes.

other angles. For the presence of vanes, the flow is accelerated towards longitudinal middle brick and gives a chance to mix with the flow passes between columns specially at $\theta = 135^{o}$. The wall effect and flow separation stands behind the obtained lowest Nusselt number for both longitudinal and transversal near wall columns when compared with the middle one. The maximum enhancement ratios differ with the brick position, brick setting, and Reynolds number.

For transverse brick in middle, the highest enhancement ratio reaches a value of 69.6% (for setting 1, attack angle 120° and Re = 23,718) while the minimum enhancement reached to about 19.1% in absence of vanes at Re = 20,236 as shown in Table 4. The maximum enhancement of relative local Nusselt number for transverse and longitudinal middle bricks takes place for settings 1 and 2, respectively for different values of attack angle. The large value of $[(Nu_{mv} - Nu_{w,nv})/Nu_{w,nv}]$ for transverse middle brick in setting 1 might be attributed to the combined effect of higher Reynolds number and turbulent vortices generated upstream the transverse middle brick for small transverse spacing between brick columns.

Fig. 8 shows the local variation of *Nu* for longitudinal brick at middle column versus Reynolds number for the investigated settings illustrated in Fig. 4 in absence and presence of vanes with the three attack angles. In absence of vanes, the highest values of local *Nu* for longitudinal middle brick are found for settings 7 and 2 whereas settings 3, 4, 1 and 5 introduce the smallest values up to Re = 26,000 as shown in Fig. 8. Settings 2 and 7 have the same columns spacing, but the middle column of setting 7 has the largest space between bricks as shown in Fig. 4. Therefore, a high blockage near wall columns enforces the air to flow on both sides of longitudinal middle brick in setting 7 which has high middle column local void fraction. Consequently, a sufficient air flow passes directly around the longitudinal middle bricks. The high resistance to flow for setting 1, 4 and 5 causes its longitudinal *Nu* to be the lowest, due to a high number of bricks which produce low local void fraction as can be seen in Table 1. As a result, it produces weak flow on the internal surface of these settings. From Fig. 8 it can be observed that the local *Nu* values of setting 7 is about 1.5 times that of setting 5 values at 120°. Although setting 3 has the highest void fraction it has a lower *Nu* for the longitudinal middle. This can be returned to the low number of bricks for same flow passages between columns which reduce the flow resistance and produces weak pore velocity within the void spaces.

The two settings pair 6, 8 and 9, 10 have a close value to each other of longitudinal local Nusselt number, as each two settings of them have the same number of bricks and void fraction. The presence of guide vanes enhances the local Nusselt number in longitudinal middle positions for all settings as shown in Fig. 8. Moreover, it can be noticed that decreasing attack angle enhances the local longitudinal middle *Nu* due to directing the flow towards the spaces in the vicinity of middle columns besides enhancing the turbulence due to the generated vortices. The average increase in longitudinal middle *Nu* for setting 7 reached about 35% in comparison with no vanes which is achieved at $\theta = 120^{o}$within $12,000 \leq Re \leq 26,000$.

2- Bricks Spacing Effect

From Fig. 8 the effect of spacing between bricks for the middle columns of settings (2 & 7, 3 & 9, and 5 & 6) can be obtained for

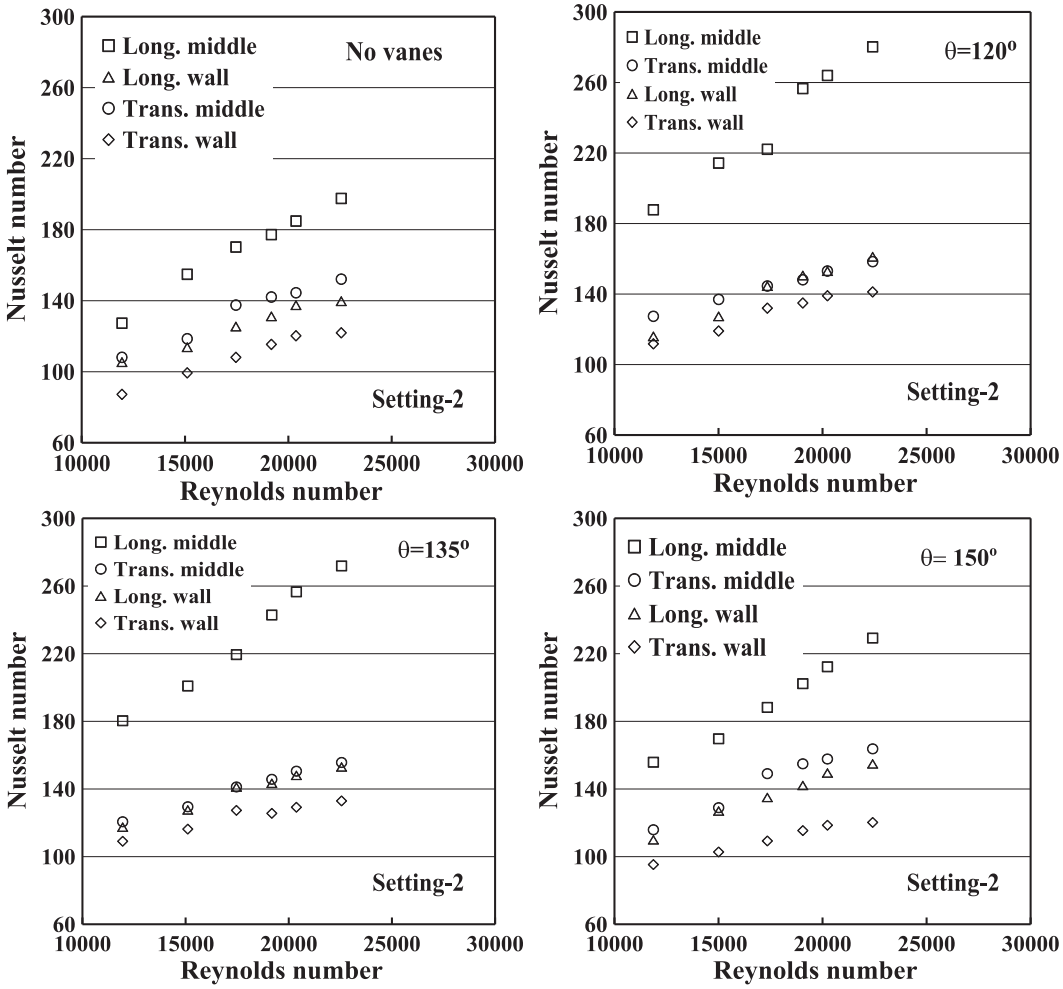

Fig. 6. Nusselt number at fifth row for three columns in setting 2.

each pair of them where all these settings have the same spacing between columns. Obviously, for settings 5 and 6, the longitudinal Nusselt number increases up to about 46% at Re = 12,000 as the space between bricks increases from 5 to 26 mm in absence of vanes. This increase depends on the setting characteristics and brick numbers. Furthermore, the presence of guide vanes provides another increase in Nusselt number as shown in Table 5. Experimental results are given in the form of percentage increasing in local Nusselt number $[(Nu_{mv,7} - Nu_{mv,2})/Nu_{mv,2}]$ where $Nu_{mv,7}$ and $Nu_{mv,2}$ are the local Nusselt numbers of longitudinal (or transversal) bricks in middle for settings 7 and 2, respectively.

For settings pair 5&6, the longitudinal middle *Nu* increases to a maximum value of 25.66%, 16.54%, and 22.79% for flow superficial velocity u_1, u_1, and u_4 and attack angle 150°, 135°, and 120°, respectively, while for same pairs of setting has a minimum values of 15.73, 10.13, and 12.6 are found at flow rate of u_5, u_3, and u_6 and attack angle 150°, 135°, and 120°, respectively. Regarding the transversal bricks, it can be noticed from Table 5B that, the enhancement is lower compared to that of longitudinal position.

3- Columns Spacing Effect

The effect of columns spacing (S) can be observed for settings 1 and 2 where these two settings have the same spacing between bricks in all columns. From Table 6 it can be seen that the longitudinal and transversal *Nu* have a maximum increase of about 26.5% and 34.5%, respectively as (S) increases from 19 to 58 mm at Re = 17,000 for no vanes. In addition to, the longitudinal *Nu* increases by about 71.9% at θ = 135° and Re = 20,000 for the presence of guide vanes. This can be attributed to the flow improvement (turbulent and accelerated flow) between columns and decrease of flow in the zone bounded by the solid bricks due to high flow resistance in channels between bricks.

6.3. Average Nusselt number

From present experimental data, the average Nusselt number is calculated for different settings arrangements with vanes for different attack angles and compared with no vanes. As shown in Fig. 9, the average *Nu* has the same trend fashion of the presented local *Nu* where settings 7 and 2 exhibits the largest average Nusselt number whereas settings 3, 4, 1, and 5 has the lowest average Nusselt number. As Reynolds number increases, the average Nusselt number increases linearly due to the decrease in boundary layer thickness, and the strong mixing of fluid in the separated region. For setting 7, the average *Nu* increases 37% over setting 5 with 40% pressure drop in Re range $12,000 \leq Re \leq 26,000$. This may be attributed to the increase of flow acceleration and turbulent.

Fig. 10 shows the effect of attack angle on the average Nusselt for settings 2 and 7. As can be noticed in Fig. 10, decreasing attack angle enhances the average *Nu* as a result of elevating the local *Nu*. The highest increase in the average *Nu* is obtained for settings 2 and 7 with vanes (θ = 120°) and reaches about 1.2 and 1.27 times values without vanes, respectively.

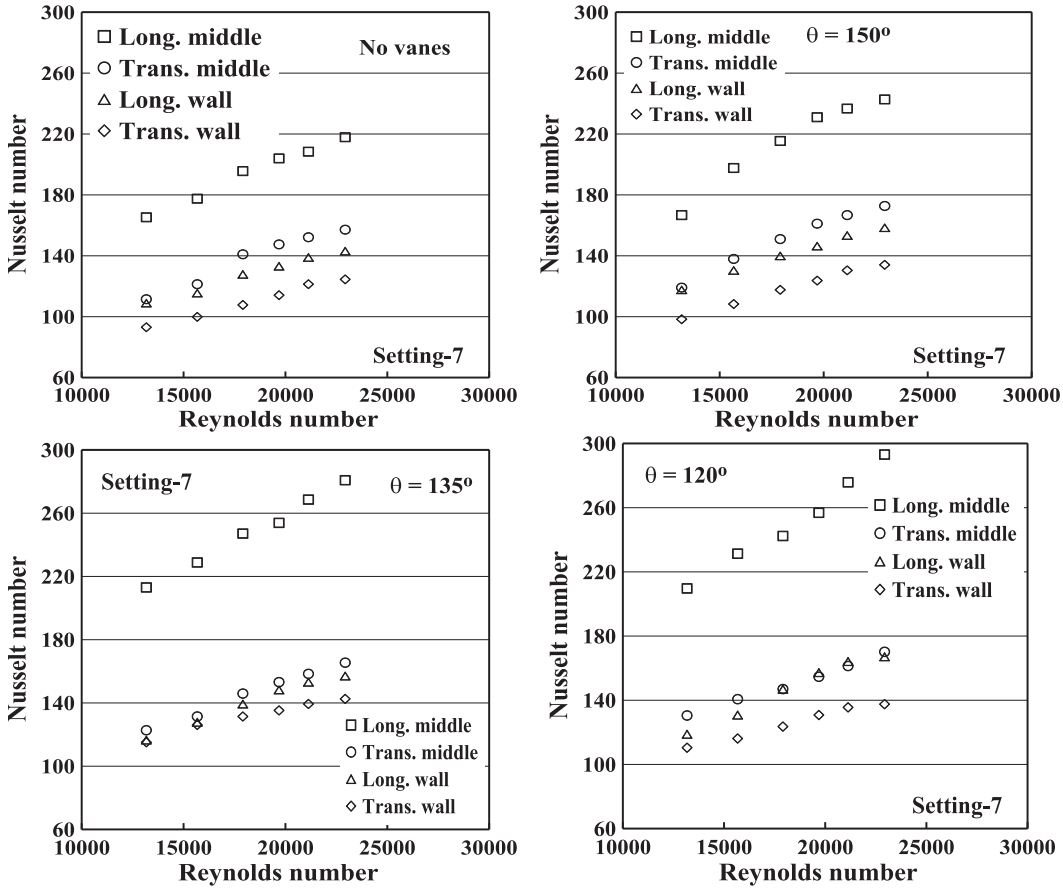

Fig. 7. Nusselt number at fifth row for three columns in setting 7.

Table 3
A maximum enhancement percentage obtained for relative local *Nu* of longitudinal brick in middle relative to wall columns.

	Setting 1		Setting 2		Setting 3		Setting 4	
	%	Re	%	Re	%	Re	%	Re
No vanes	43	23,718	41.4	22,407	25.7	25,821	5.4	24,956
θ =150°	47.1	23,718	64.0	22,407	36.0	20,236	12.2	24,956
θ =135°	57.1	23,718	94.5	22,407	45.1	22,150	13.9	14,204
θ =120°	62.3	23,718	83.5	22,407	48.5	20,236	27.3	21,404

Table 4
A maximum enhancement percentage obtained for relative local *Nu* of transverse brick in middle relative to wall columns.

	Setting 1		Setting 2		Setting 3		Setting 4	
	%	Re	%	Re	%	Re	%	Re
No vanes	29.6	23,718	24.8	22,407	27.3	25,821	22.9	24,956
θ =150°	57.7	21,609	34.3	22,407	19.1	20,236	22.9	19,468
θ =135°	65.2	23,718	38.2	11,867	53.8	25,821	23.8	24,956
θ =120°	69.6	23,718	45.9	11,867	53.9	20,236	27.2	24,956

6.4. Average rate of heat exchange

The kiln productivity depends on the average Nusselt number if only there is the same number of bricks. The kiln productivity is related to the actual rate of heat transfer between combustion gases or air to/from bricks. So that, for the ideal case (no heat loss and no radiation effects), the kiln productivity is given by (Qave = havAw; bΔT) as presented in Ref. [15]. Fig. 11 represents average heat exchanged between air and bricks for all settings with a temperature difference of 1 K as a function in mass flux. Fig. 11 illustrates the effect of mass velocity (M) on the heat transfer rate (Q_{ave}) for different settings and attack angles. It can be noticed that the average rate of heat transfer has its highest values at settings 2 and 7 for all cases with and without guide vanes for mass velocity ranged from 4 kg/(m^2.s) to 8 kg/(m^2.s). The highest enhancement in the heat transfer rate is observed for setting 2 with an angle of attack 120° and mass velocity 8 kg/m^2.s compared with setting with no vanes. This can be attributed to the higher average Nusselt number values and a moderate void fraction. Moreover, setting 3 has the lowest average rate of heat transfer, because it has the higher value of void fraction and a low number of bricks as shown in Fig. 11. In addition to, as the attack angle of guide vanes decreases the average heat transfer rate increases for all studied settings as shown in Fig. 11. So it can be concluded that the kilns which use settings 2 and 7 has the shortest production time but lowest productivity. On the other hand, kilns which use settings 1, 4 and 5 in presence of guide vanes have the highest productivity and moderate production time.

Fig. 12 demonstrates the effect of guide vanes attack angle on the average rate of heat exchange for settings 2 and 7. It is found that as the attack angle of the guide vanes decreases the average rate of heat exchanges increases due to the increase in the average *Nu* presented in Fig. 10. For a given mass velocity, the average rate of heat exchange in presence of guide vanes with an attack angle of 120° have a value higher than that with attack angles 135° and 150° due to the turbulence improvement and flow acceleration.

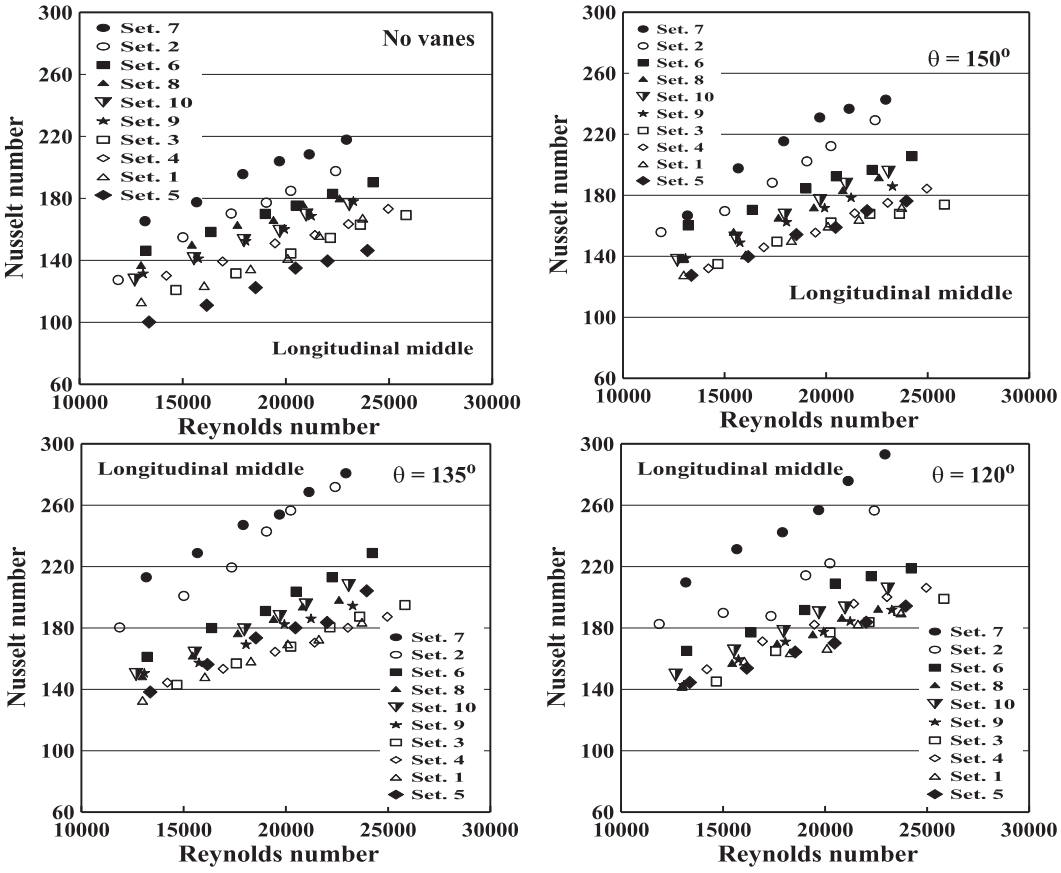

Fig. 8. Longitudinal *Nu* versus Re for the middle column of the different settings.

Table 5
Percentage increasing in local Nusselt number as brick spacing changes from 5 to 26 mm.

A (longitudinal middle)												
Flow velocity, u	No vanes			θ=150°			θ=135°			θ =120°		
	7&2	9&3	5&6	7&2	7&2	9&3	5&6	7&2	7&2	9&3	5&6	7&2
u_1	29.79	8.67	45.90	7.00	2.72	25.66	18.13	5.27	16.54	14.83	1.68	14.22
u_2	14.62	7.19	42.57	16.51	0.45	21.92	13.90	0.22	15.17	21.87	3.42	15.17
u_3	14.94	5.48	38.89	14.45	0.11	19.62	12.61	0.78	10.13	29.07	3.55	16.67
u_4	15.08	3.59	29.87	14.21	2.27	21.04	4.54	1.10	13.07	19.85	3.62	22.79
u_5	12.74	3.40	30.99	11.52	6.32	15.73	4.70	0.74	16.01	24.16	3.70	16.33
u_6	10.26	5.19	30.10	5.88	6.85	16.70	3.30	0.29	12.06	14.26	3.78	12.60
B (Transversal middle)												
Flow velocity, u	**No vanes**			**θ=150°**			**θ =135°**			**θ =120°**		
	7&2	**9&3**	**5&6**	**7&2**	**9&3**	**5&6**	**7&2**	**9&3**	**5&6**	**7&2**	**9&3**	**5&6**
u_1	3.10	6.00	6.97	2.75	1.06	3.13	1.75	2.34	4.00	2.46	0.45	5.96
u_2	2.35	8.49	7.11	6.98	2.86	6.26	1.51	3.10	7.13	2.71	0.32	7.32
u_3	2.50	9.96	3.48	1.28	3.97	7.75	3.36	0.05	10.67	1.65	3.15	6.47
u_4	3.80	8.63	3.06	4.03	2.47	6.51	5.12	1.39	8.79	4.44	3.19	4.34
u_5	5.33	8.69	3.05	5.71	2.35	8.62	5.23	4.29	6.66	5.41	3.24	5.71
u_6	3.30	10.37	4.13	5.50	3.73	6.40	6.30	5.58	3.39	7.44	3.31	6.82

6.5. Performance criteria

To evaluate the performance benefits of the refractory materials firing with different setting arrangements at constraint of equal pumping power was applied. The pressure drop across the setting arrangement must be taken into consideration for equal pumping power constraint across the heat transfer process. Therefore, the pressure drop is more significant regarding heat transfer enhancement for equal pumping power than that for equal mass flow rate.

Combining the experimentally determined friction factor of the enhanced configuration (setting with vanes) and those of the setting in absence of the vanes, an equation gives a relation for constant pumping power [31–33];

Table 6
Percentage increasing in Nusselt number as columns spacing changes from 19 to 58 mm.

Flow velocity, u	No vanes		θ =150º		θ =135º		θ =120º	
	Long.	Trans.	Long.	Trans.	Long.	Trans.	Long.	Trans.
u_1	12.44	20.84	37.58	29.53	59.23	34.82	61.22	42.36
u_2	25.21	23.68	37.15	34.50	62.41	35.07	53.47	42.86
u_3	26.51	34.50	39.90	45.77	63.10	38.08	39.56	41.37
u_4	25.45	32.33	43.17	44.25	71.90	35.71	51.68	37.92
u_5	18.45	29.71	36.00	41.61	64.39	35.15	42.33	37.42
u_6	18.16	31.78	37.06	41.82	62.55	34.84	53.40	37.19

$$\eta = \frac{Nu/Nu_o}{(f/f_o)^{1/3}} \tag{15}$$

To keep the pumping power constant, the flow velocity for setting without vanes must be increased. The pumping power required to feed the fluid flow through the setting brick module is proportional to Reynolds number. The combined effects of vane attack angle and Reynolds number on the Nusselt number and friction factor ratio at constant pumping power are shown in Fig. 13. It can be observed that the dependence of (η) on the setting arrangement and vane angle is more significant while the dependence on Re is a small significant effect. Also, it is obvious that the performance criteria (η), is greater than one for setting 1 and 2 and increases with decreasing attack angle over the investigated Reynolds number range. The increase in the performance criteria reaches about 15% for settings 1 and 2 as shown in Fig. 13. However, attached vanes enhance the average *Nu* as shown in Fig. 8, the accompanied increase in pressure drop exceeds this enhancement as illustrated in the following figure for settings 3 to 10. The maximum decrease in the performance criteria reaches about 30% at Re = 12,000 for setting 3 at θ = 120º.

6.6. Experimental correlation

Finally, an empirical correlation is obtained for the average Nusselt number *Nu* in terms of Reynolds number (Re), brick setting dimensionless groups (S/a), (εS/b), and angle of attack (θ) as follows:

$$Nu = 1.617Re^{0.42}\left(\frac{S}{a}\right)^{-0.147}\left(\varepsilon\,\frac{S}{b}\right)^{0.224}\left(\frac{\theta}{180}\right)^{-0.39} \tag{16}$$

This correlation satisfies the present experimental data within ±15% maximum deviation as shown in Fig. 14 for the ranges of Reynolds number (11,867 ≤ Re ≤ 25,821), and setting characteristics ratios (0.33 ≤ (S/a) ≤ 1.0), (0.79 ≤ (εS/b) ≤ 3.0), and (120º ≤ θ ≤ 180º).

7. Conclusions

An experimental test section is conducted in the present work to

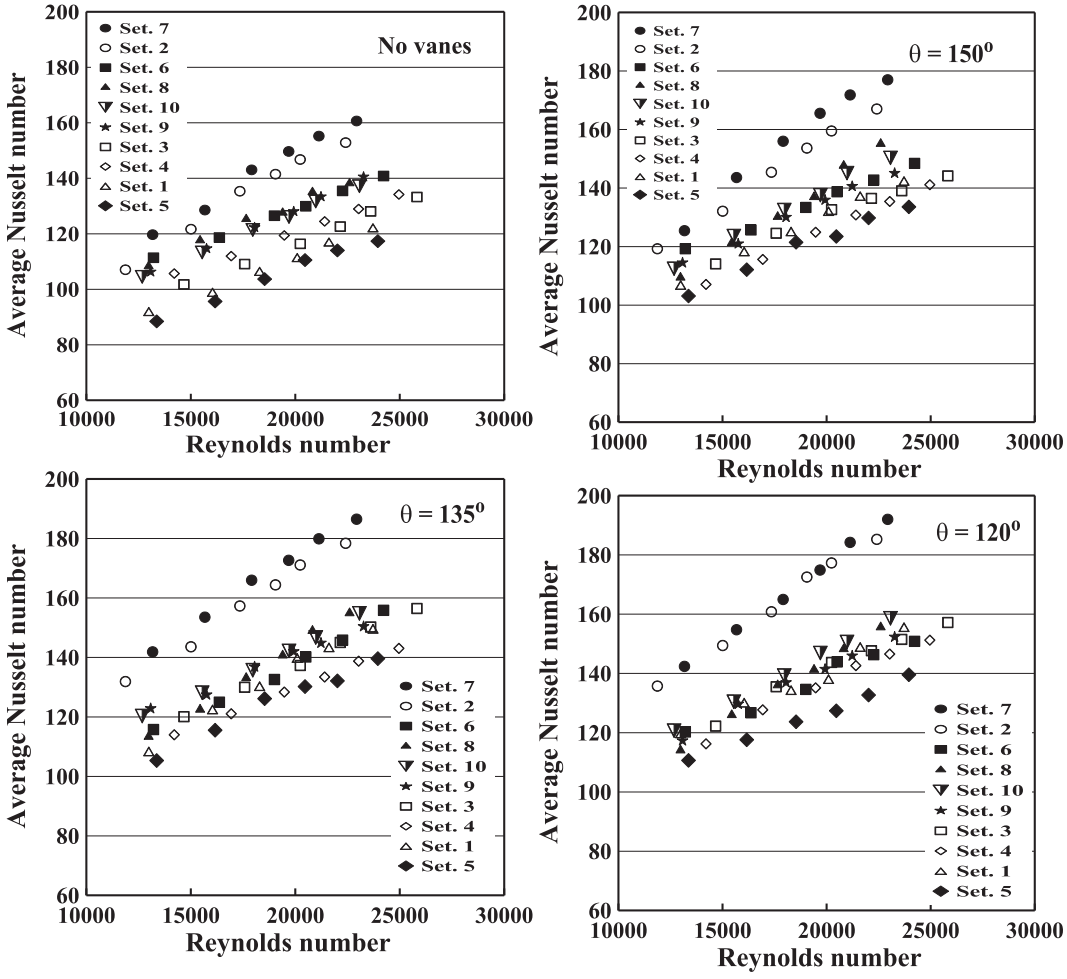

Fig. 9. Average *Nu* versus Re for all studied settings with the three different vanes angles.

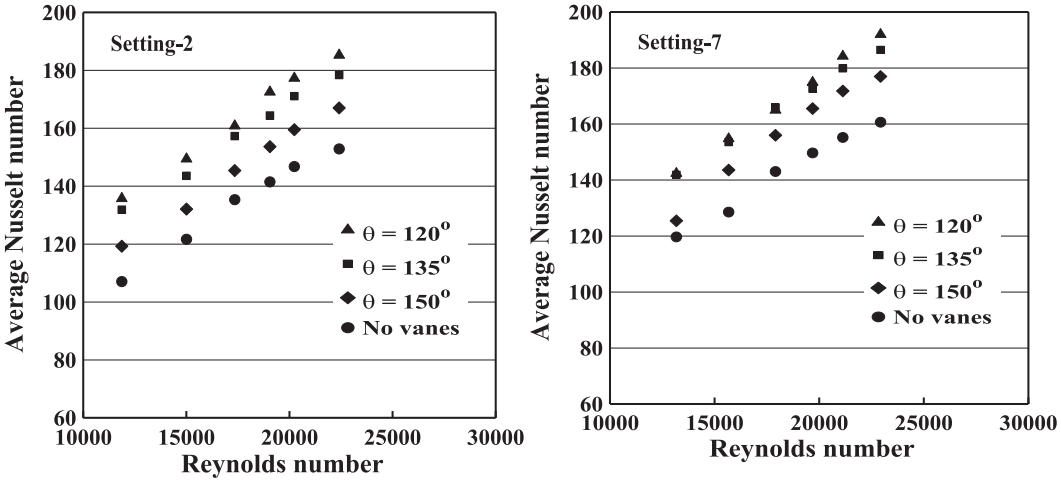

Fig. 10. Average *Nu* versus Re for settings 2, 7 with the three different vanes angles.

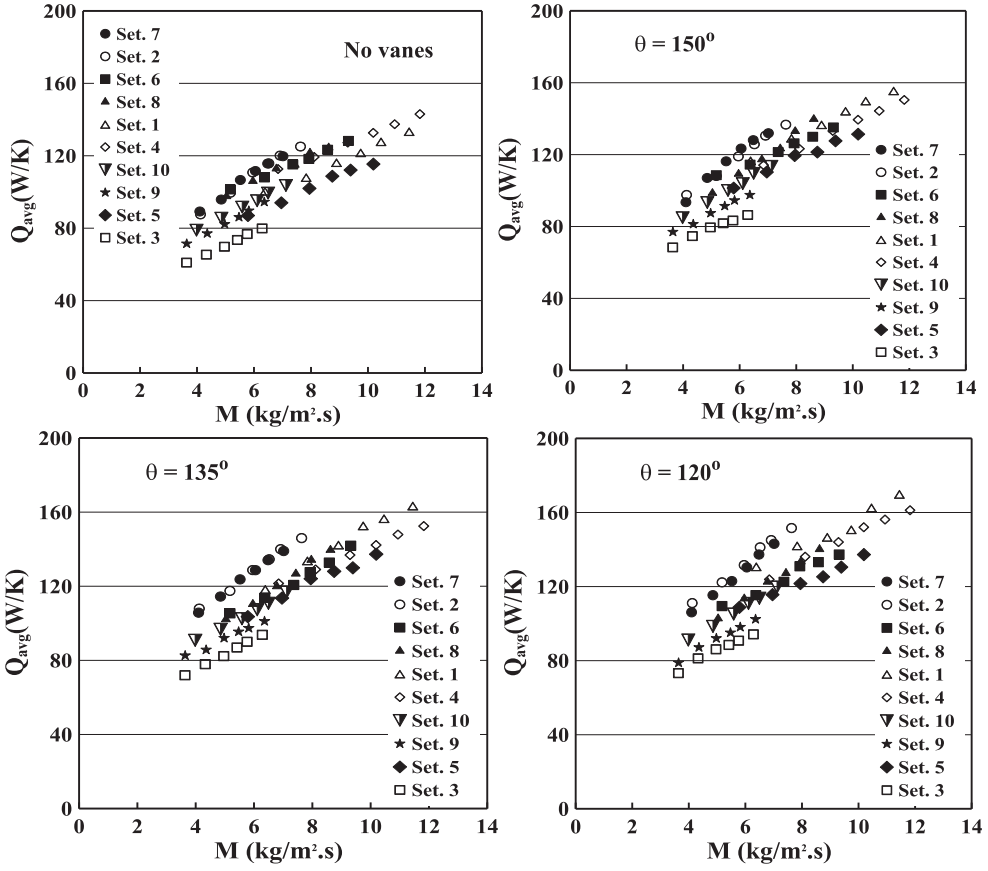

Fig. 11. Average heat transfer rate for all studied settings and vanes angles versus M.

simulate the cooling zone of a tunnel kiln. An experimental investigation of heat transfer and pressure drop is done to ten different brick settings. In addition to, an augmentation technique using guide vanes with attack angles120°, 135° and 150° attached to the kiln side walls is presented. The experimental results revealed that:

- For all studied settings, Nusselt numbers in the longitudinal direction are larger than Nusselt numbers in transversal one without and with attack angles.
- The attack angle has a great influence on the average Nusselt number for all settings. Decreasing the attack angle enhances the average Nusselt number as a result of elevating the local Nusselt number.

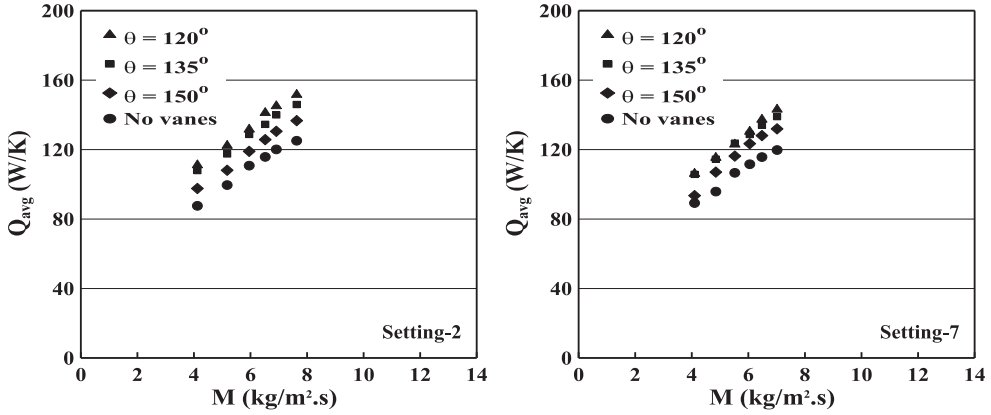

Fig. 12. Effect of guided vanes angle on the average heat transfer rate for settings 2 and 7.

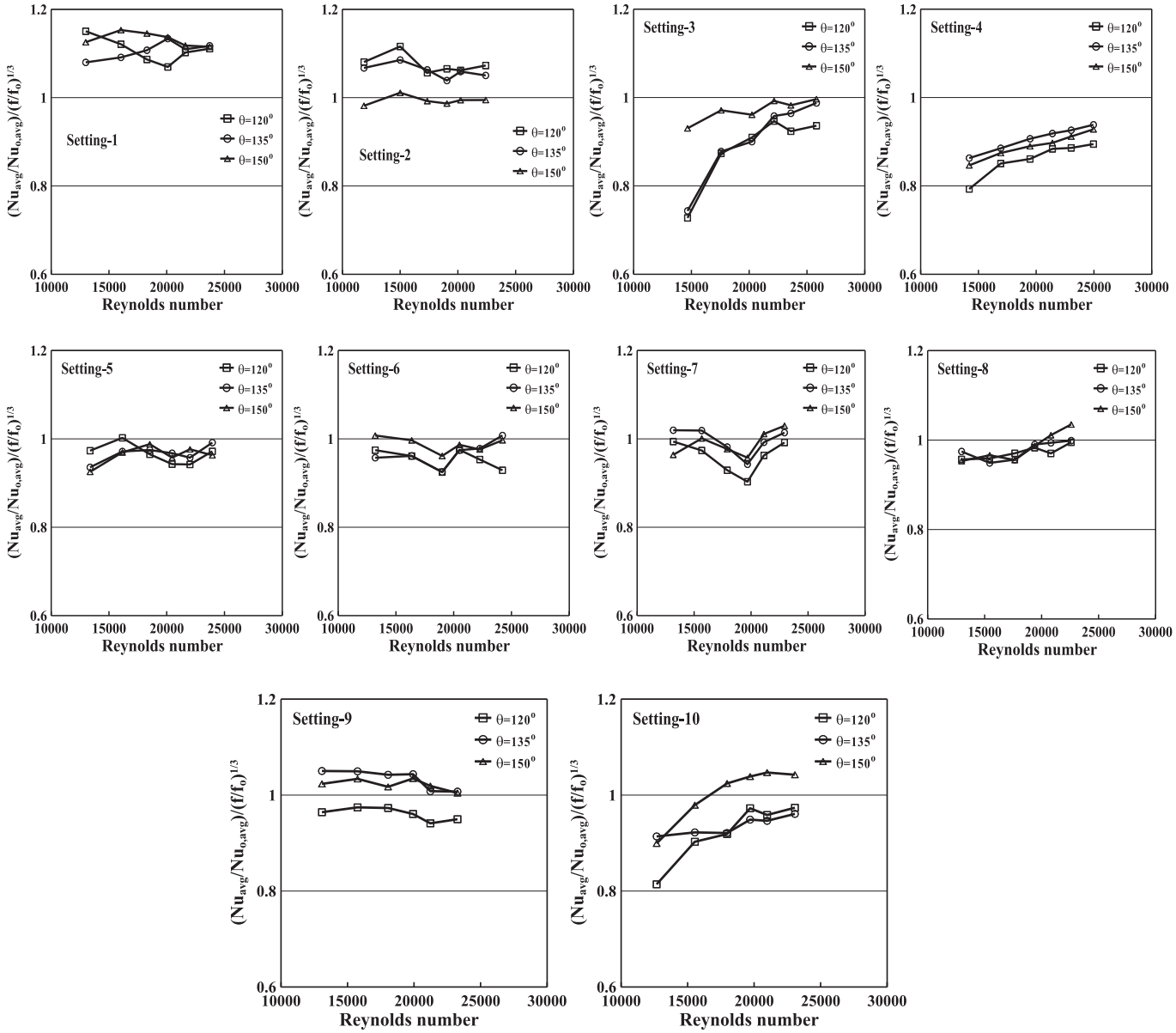

Fig. 13. Performance criteria versus Reynolds number for the different investigated settings.

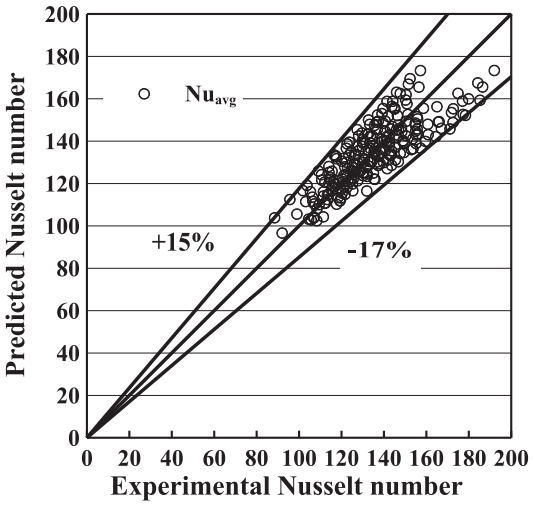

Fig. 14. Correlated Nusselt number versus experimental Nusselt number.

- As the space between bricks increases from 5 to 26 mm the longitudinal Nusselt number increases for all cases with and without vanes and it depends on the setting characteristics and brick numbers.
- As the space between columns increases from 19 to 58 mm in absence of vanes, the longitudinal and transversal Nusselt numbers increase by about 26.51% and 34.5%, respectively at Re = 17,000.
- In presence of guide vanes, the maximum enhancement in relative local Nusselt number reaches to about 94.5% at $\theta = 135^{o}$ and Re = 20,000 for the longitudinal middle brick.
- As Reynolds number increases the average Nusselt number almost increases linearly. Furthermore, the amount of increase depends up on the setting characteristics.
- The highest enhancement in the heat transfer rate is observed for setting 2 with angle of attack 120° and mass velocity 8 kg/m^2.s compared with setting with no vanes.
- In addition to, the guide vanes increases the average heat rate as the attack angle decreases for all studied settings. So it can be concluded that, the kilns which use settings 2 and 7 has the shortest production time but lowest productivity. On the other hand, kilns which use settings 1, 4 and 5 have highest productivity and moderate production time.
- The increase in the performance criteria reaches about 15% for settings 1 and 2. However, attached vanes enhances the average Nusselt number and the maximum decrease in the performance criteria reaches about 30% at Re = 12,000 for setting 3 at $\theta = 120^{o}$.
- An empirical correlation is obtained for the average Nusselt number (Nu) terms of Reynolds number (Re), brick setting dimensionless groups ($\frac{S}{a}$), ($\varepsilon\frac{S}{b}$), and angle of attack (θ) within $11{,}867 \leq Re \leq 25{,}821$, $0.33 \leq (\frac{S}{a}) \leq 1.0$, $0.79 \leq (\varepsilon\frac{S}{b}) \leq 3.0$) and ($120^{o} \leq \theta \leq 180^{o}$).
- For brick industry application that normally requires much greater electric power, the heat transfer augmentation can be selected for different settings with using combustion gases that can compete with current electric kilns. Artificially increasing the heat transfer coefficient can greatly reduce the production time and consequently, increase the productivity. In conclusion, the augmentation heat transfer technique used in tunnel kiln based on combustion is competitive in terms of operating cost especially for industrial applications.

References

[1] Refaey HA. Mathematical model to analyze the heat transfer in tunnel kilns for burning of ceramics. Ph.D. dissertation. Magdeburg, Germany: Otto- von Guericke University; 2013.
[2] Meng P. Solid-solid recuperation to improve the energy of tunnel kiln. Ph.D. dissertation. Magdeburg, Germany: Otto von Guericke University; 2011.
[3] Lingl H. Innovative prospects for the firing technique in the production of backing bricks. Keramische-Zeitschrift 1998;50(10):4–8.
[4] Ryan JD. Practical applications of pulse firing in tunnel kilns for the structural clay industry. Ceram Eng Sci Proc 1997;18(2):367–73.
[5] Boming YU. Dynamic modeling of tunnel kiln. Heat Transf Eng 1994;15(2):39–53.
[6] Merienne J. Tunnel kilns with liquid seal. Ziegelind Int 1994;47(10):674–7.
[7] Ketels U. Possibilities for obtaining uniform temperature distribution in the tunnel kiln setting. Ziegelind Int 1990;43(7):410–9.
[8] Riedel R. False air and convection in tunnel kilns. Ziegelind Int 1989;42(6):310–6.
[9] Dugwell DR, Oakley DE. Correlation of convective heat transfer data for tunnel kilns. J Inst Energy 1988;61:165–71.
[10] Denissen J, Vries AH, Fifer J, Lowe A. Reduction of fluoride emission from clay material. Ziegelind Int 1998;51(1–2):19–26.
[11] Pariyar SK, Ferdous TDT. Environment and health impact for brick kilns in kathmandu valley. Int J Sci Technol Res 2013;2(5):184–7.
[12] Tehzeeb AH, Bhuiyan M, Jayasuriya N. Evaluation of brick Kiln performances using computational fluid dynamics (CFD). Energy Environ Eng J 2012;1(2):86–93.
[13] Dugwell DR, Oakley DE. A model of heat transfer in tunnel kilns used for firing refractories. Int J Heat Mass Transf 1988;31(11):2381–90.
[14] Karaush SA, Chizhik YI, Bober EG. Optimization of ceramic setting as a function of their heat absorption from the radiating walls of the furnace. Glass Ceram 1997;54(5):190–2.
[15] Abou-Ziyan HZ. Convective heat transfer from different brick arrangements in tunnel kilns. Appl Therm Eng 2004;24:171–91.
[16] Riedel R. The optimization of tunnel kilns by utilization of convection. Ziegelind Int 1989;42(7–8):373–9.
[17] Carvalho MG, Nogueira M. Improvement of energy efficiency in glass-melting furnaces, cement kilns and baking ovens. Appl Therm Eng 1997;17(8–10):921–33.
[18] Gao J. Production practice of super high temperature tunnel kiln with energy saving. Iron Steel 1994;29(11):64–7.
[19] Roth H. Combined heating and power systems in brickworks. Ziegelind Int 1993;46(9):545–52.
[20] Almeida GS, Silva JB, Silva CJ, Swarnakar R, Neves GA, Lima AG. Heat and mass transport in an industrial tunnel dryer: modeling and simulation applied to hollow bricks. Appl Therm Eng 2013;55:78–86.
[21] Refaey HA, Specht E. Flow field visualization to simulate the burning of sanitaryware in tunnel kilns. In: Proceedings of ICFD11: eleventh international conference of fluid dynamics december 19-21; 2013 [Alexandria, Egypt].
[22] Mancuhan E, Kucukada K, Alpman E. Mathematical modeling and simulation of the preheating zone of a tunnel kiln. J Therm Sci Technol 2011;31(2):79–86.
[23] Kaya S, Kucukada K, Mancuhan E. Model-based optimization of heat recovery in the cooling zone of a tunnel kiln. Appl Therm Eng 2008;28:633–41.
[24] de Paulo Nicolau V, Dadam AP. Numerical and experimental thermal analysis of a tunnel Kiln used in ceramic production. J Braz Soc Mech Sci Eng 2009;31(4):297–304.
[25] Durakovic J, Delalic S. Temperature field analysis of tunnel kiln for brick production. Mater Geoenvironment 2006;53(3):403–8.
[26] Naccache MF, Gomes MSP, Nieckele AO. Numerical simulation of flow and heat transfer through a tunnel Kiln. In: 18th international congress of mechanical engineering november 6-11; 2005. Ouro Preto, MG.
[27] Essenhigh RH. Studies in Furnace Analysis: prediction of tunnel Kiln performance by application of the integral energy equation. Energy & Fuels 2001;15(3):552–8.
[28] Santos GM. Study of thermal behavior of a tunnel kiln used in red ceramic industry. M.Sc. dissertation. Santa Catarina, Brazil: Federal University of Santa Catarina; 2001. in portuguese.
[29] Refaey HA, Specht E, Salem MR. Influence of fuel distribution and heat transfer on energy consumption in tunnel Kilns. Int J Adv Eng Technol 2015;8(3):281–93.
[30] Kline SJ, McClintock FA. Describing uncertainties in single-sample experiments. Mech Eng 1953;75(1):3–8.
[31] Webb RL. Performance evaluation criteria for use of enhanced heat transfer surfaces in heat exchanger design. Int J Heat Mass Transf 1981;24:715–26.
[32] Webb RL, Eckert ERG. Application of rough surface to heat exchange design. Int J Heat Mass Transf 1972;15:1647–58.
[33] Fan JF, Ding WK, Zhang JF, He YL, Tao WQ. A performance evaluation plot of enhanced heat transfer techniques oriented for 0 energy-saving. Int J Heat Mass Transf 2009;52(2):33–4.